Article

Determining Feature Based Hydraulic Geometry and Rating Curves using a Physically Based, Computationally Efficient Framework

J. Michael Johnson[1, 2*], Jim Coll[1], Keith Clarke[2], Shahab Afshari[3,4], Siddharth Saksena[5], Lilit Yeghiazarian[6]

[1]Lynker, Fort Collins, Colorado, USA
[2]Department of Geography, University of Santa Barbara, Santa Barbara, California, USA
[3]Department of Civil Engineering and Environmental Engineering, Virginia Tech, Blacksburg, Virginia, USA
[4]Department of Geosciences, University of Massachusetts, Amherst, Massachusetts, USA
[5]Department of Civil and Environmental Engineering, University of Massachusetts, Amherst, Massachusetts, USA
[6]Department of Chemical and Environmental Engineering, University of Cincinnati, Cincinnati, Ohio, USA
* Correspondence: jjohnson@lynker.com

Abstract: Hydraulic relationships are important for water resource management, hazard prediction, and modelling. Since Leopold first identified power law expressions that could relate streamflow to top-width, depth, and velocity, hydrologists have been estimating 'At-a-station Hydraulic Geometries' (AHG) to describe average flow hydraulics. As the amount of data, data sources, and application needs increase, the ability to apply, integrate and compare disparate and often noisy data is critical for applications ranging from reach to continental scales. However, even with quality data, the standard practice of solving each AHG relationship independently can lead to solutions that fail to conserve mass. The challenge addressed here is how to extend the physical properties of the AHG relations, while improving the way they are hydrologically addressed and fit. We present a framework for minimizing error while ensuring mass conservation at reach - or *hydrologic Feature* - scale geometries'(FHG) that complies with current state-of-the-practice conceptual and logical models. Through this framework, FHG relations are fit for the United States Geological Survey's (USGS) Rating Curve database, the USGS HYDRoacoustic dataset in support of the Surface Water Oceanographic Topography satellite mission (HYDRoSWOT), and the hydraulic property tables produced as part of the NOAA/Oakridge Continental Flood Inundation Mapping framework. The paper describes and demonstrates the accuracy, interoperability, and application of these relationships to flood modelling and presents this framework in an R package.

Keywords: hydraulic geometry; rating curves; flood modelling; accuracy; data acquisition; data usability; data interoperability; data needs

1. Introduction

River systems are critical to model and measure but are notoriously complex. Simplified hydraulic geometry can be used to represent average conditions and reduce the need for detailed field surveys as well as the computational burden while studying and modelling river dynamics [1]. In hydraulic theory, streamflow (Q), top-width (TW), depth (Y), and velocity (U) are inherently related and describe how water moves through a channel [2], and in the abstract sense, the shape of the channel [3]. The focus on a single location is referred to as 'at-a-station hydraulic geometry' (AHG) and can be represented as a set of power law equations under the assumption of steady-state continuity:

$$\begin{aligned} Q &= TW \times Y \times U \\ &= aQ^b \times cQ^f \times kQ^m \\ &= ack \times Q^{b+f+m} \end{aligned}$$

Preprints (www.preprints.org) | NOT PEER-REVIEWED | Posted: 21 December 2022 doi:10.20944/preprints202212.0390.v1

(1)

where TW is top-width, Y is the mean depth, and U is the velocity resulting from streamflow Q. Thus, each relation can be described as:

$$TW = aQ^b \quad (2)$$

$$Y = cQ^f \quad (3)$$

$$U = kQ^m \quad (4)$$

and, given the continuity relation of Equation 1, an idealized system meets the following constraints:

$$a \times c \times k = 1 \quad (5)$$

$$b + f + m = 1 \quad (6)$$

When either continuity constraint is violated, it implies an artificial gain or loss of water in the system [1–3].

Many geomorphic, hydraulic, water quality, and river navigation processes are functions of these hydraulic states. As such, AHG relationships have proven useful for determining a range of critical discharge values [4] and support efforts including flood routing [5,6], riverine-habitat analysis [7], water-quality management, reservoir-sedimentation, and sediment movement studies [3].

The depth relation (Equation 3) in particular has enormous practical application as the empirical c and f terms represent the traditional calibrated rating-curve method used by the United States Geological Survey (USGS) and other water-monitoring agencies [8,9]. To be a true "rating curve", however, the mean depth relation is often reported with respect to a reference elevation - or datum - modifying the equation to be:

$$Q = \alpha\ (h - h_o)^{\beta} \quad (7)$$

where h_o is a reference elevation and h is the measured height of water for a given streamflow (Q).

In a wide range of cases, hydraulic data is not reported in the power law notation but rather as a set of tables relating values of Q to values of one or more hydraulic response variables. Thus, the relationships available to end users require lookup and interpolation across these tables or require the power law relationships to be fit - a process that generally relies on an Ordinary Least Squares (OLS) regression fit over log transformed values.

Modern efforts to supply real-time flood extent forecasts for the continental USA (Johnson et al., 2022; Y. Y. Liu et al., 2018; Maidment, 2016) rely heavily on a streamflow-depth conversion based on rating curves that are normalized to the elevation of the local river channel [13]. In these workflows, the translation of millions of Q values to Y values using rating tables is a major bottleneck. There is therefore a unique opportunity for AHG relationships to efficiently provide critical information, while also exploring probabilistic rating relationships. Motivated by this use case, a large part of this research focuses on the streamflow-depth rating curve relationship. In these same applications there is a need for improved channel geometry estimation [14] and hydraulic routing (t-route; https://github.com/NOAA-OWP/t-route). The system based AHG relationships offer a

 doi:10.20944/preprints202212.0390.v1

unique opportunity for parameterizing a more realistic and computationally efficient channel shape [3].

1.1. Theory and Data

While the AHG power laws provide an elegant theory for representing a mass-constrained hydraulic system, the data available to determine these relations are rarely as clean. Rating relationships are time varying and associated with a large amount of variation and error [15,16]. This becomes more relevant as data currently are not only collected in the field but also using automated techniques and models. For example, river top widths can be extracted from aerial imagery [17–19]; synthetic rating curves can be estimated from digital elevation models [11,20]; and an increasing diversity of sensors are being deployed to capture in-situ and remote readings [21,22]. In each of these cases, the distribution, database design, and lack of uniformity make working with tables a difficult and computationally intensive process.

An overlooked aspect of increasingly diverse data (size and type) is that even if data are available in a way to fit AHG relationships, the traditional OLS approaches do not necessarily provide the most accurate fit and cannot enforce the continuity (Equations 5-6) present in the theoretical hydraulic system the same ways nonlinear and evolutionary algorithm approaches can.

Afshari et al. (2017) was one of the first to consider this issue when they approximated AHG relations for ~4,000 field surveys in the USGS "HYDRoacoustic dataset in support of the Surface Water Oceanographic Topography satellite" mission (HYDRoSWOT) dataset [23]. In doing this, they found a principal challenge was the uncertainty in measurements of dynamic river systems over long periods of time. As a result, they proposed a statistical data filtering method based on a recursive Modified Cross-Validation and Regression Diagnostics to remove potential outliers prior to fitting power law relations. Their work marked the first instance of a "feature engineering" approach being applied to AHG relations; however, the methods were computationally expensive and difficult to reproduce making it challenging to extend to new data. Furthermore, in evaluating the results, many sites still failed to meet the continuity constraints within a +/-0.05 allowance, suggesting that data cleaning on its own is not enough to ensure valid solutions. Thus, a principal goal of this research is to evaluate candidate curve fitting methods that can handle noisy input data to provide valid, mass conserving, analytical solutions.

1.2. At-a-Station vs At-a-Feature

Not all measurements occur at the exact same location while they might represent the same holistic hydrologic feature. For example, the Open Geospatial Consortium HY Features Conceptual model defines a catchment as a physiographic unit where hydrologic processes take place. Such a unit is defined by a hydrologically determined outlet to which all water flows. In this context a feature is a scale-dependent unit of hydrology, and, depending on the desired scale, can be a set of incremental flowpath and catchment divides, or a set of continuous drainage basins [24].

Hydrologic addresses link a hydrologic network (set of flowpaths and divides) to any data that can be idealized as a point (XY) location [25,26]. Once addressed to the network, a wide range of practical applications can be carried out, including but not limited to network navigation, network accumulation, and river identification. Therefore, being able to hydrologically address a relationship to a particular hydrologic feature makes the discovery, integration, and inference of relationships more feasible. If a highly resolved reference network (e.g. the NHDPlusV2 [27], USGS reference network [28], NOAA Next Generation Water Modelling Framework network [29] or a global dataset [30]) is chosen, then the "at-a-station" and "at-a-feature" hydraulic geometries (respectively AHG and FHG) could be used interchangeably.

Preprints (www.preprints.org) | NOT PEER-REVIEWED | Posted: 21 December 2022 doi:10.20944/preprints202212.0390.v1

1.3. Role in Hydrologic Applications

While there is scientific interest in identifying more robust ways to accurately describe a hydraulic system with respect to reference hydrologic features, there is equal practical interest in demonstrating the advantages of concise power law relationships in modern hydrologic applications such as rating curves estimation [20]; flood forecasting [10,13] and flood warning [31–33]. These advantages are highlighted in the discussion and include that they:

- Are more efficient and reproducible to use then table-based lookup and interpolation approaches.
- Are easier to compare across different sources
- Facilitate data requests at "single site" or "many sites" - a challenge that exists in time series and table-based databases like National Water Information System (NWIS) (streamflow and rating curves) and Continental Flood Inundation Mapping (CFIM) (rating curves).
- Provide an opportunity to represent uncertainty through multiple realizations per feature
- Provide learnable parameters that are essential to estimating hydraulic shape and behavior at unmonitored locations using data driven methods

The focus of this work is to provide a reproducible fitting framework that provides hydrologic addressing while minimizing error and enforcing continuity when possible. The *data* section introduces the three datasets being tested which include the USGS rating curves, the USGS HYDRoSWOT dataset, and the CFIMs Synthetic Rating Curves (SRCs). The *methods* section describes the fitting approaches; how rating relationships can be compared; and how hydraulic systems can be evaluated as a multi-objective optimization problem. The *results* highlight the error introduced by these fitting methods and compare the results to the statistical data filtering approaches put forth in Afshari, 2017. Lastly, in the *discussion* we illustrate examples that highlight the performance and practical gains of this approach in areas of flood forecasting, uncertainty representation, and machine learning.

2. Materials and Methods

2.1. Data

2.1.1. USGS Rating Curves

The USGS provides rating curve relations through the National Water Information System (NWIS). USGS rating curves can be accessed by NWIS site ID using the *dataRetrieval* R package [34]. These ratings describe water depth in relation to an arbitrary and inconsistent elevation (datum), thus height is relative rather than absolute. For this study, 7,532 ratings tables were identified with record counts ranging from 22 to 7,466 (with a mean of 1,488) observations per station. Stage values were converted to meters and then depths (h) by subtracting the reported zero-flow stage ($\sim h_o$) from all values (approximating equation 7).

2.1.2. USGS HYDRoSWOT Field Measurements

At a smaller number of sites, the USGS maintains field surveys as part of the USGS "HYDRoacoustic dataset in support of the Surface Water Oceanographic Topography satellite" mission (HYDRoSWOT). This dataset stores a long record of manually recorded top width (TW), velocity (U), channel area (A) and discharge (Q) values for a number of locations across the USA [23]. For this study, 3,544 gauge locations with at least 50 unique measurements over at least 30 years were identified. Channel area (A) was converted to a mean depth (Y) by dividing by the top width (TW). Figure 1 shows the geographic distribution of these stations and type of records available.

Preprints (www.preprints.org) | NOT PEER-REVIEWED | Posted: 21 December 2022 doi:10.20944/preprints202212.0390.v1

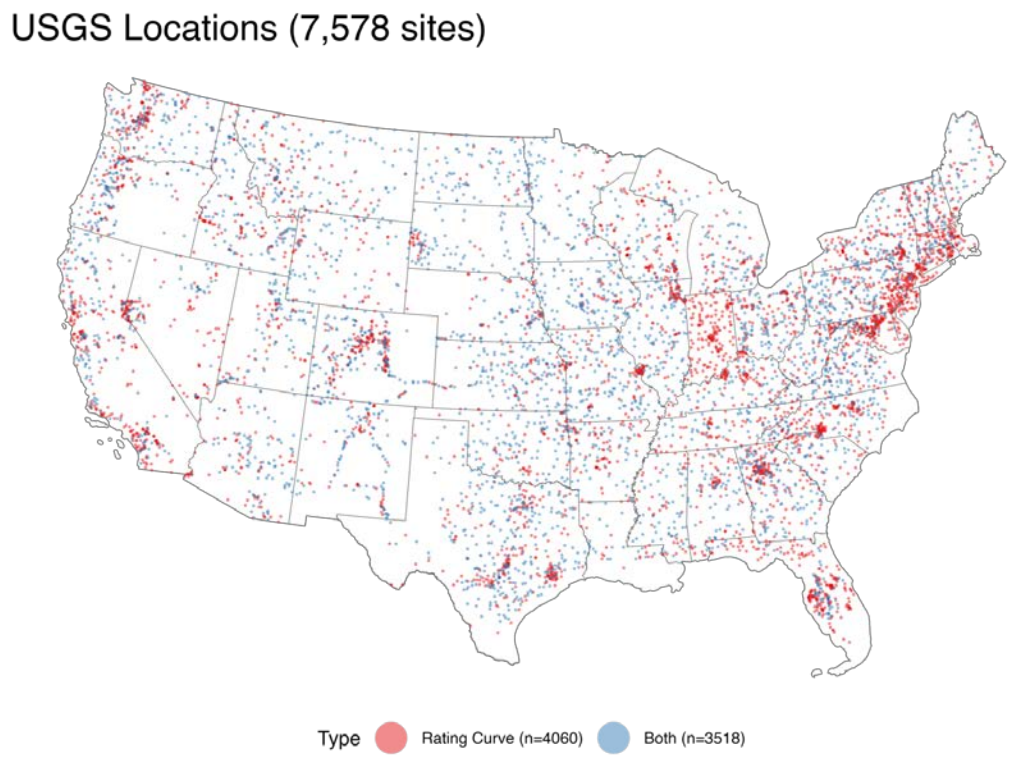

Figure 1. The 3,518 USGS monitoring locations with field measurements with at least 50 hydraulic (Q, TW, U, Y) observations over the last 30 years and the 7,578 USGS gages with active rating curve measurements

2.1.3. Continental Flood Inundation Mapping (CFIM) Hydraulic Property Tables

In 2016 the NOAA Office of Water Prediction operationalized the National Water Model to forecast streamflow and other hydrologic states across the Continental USA (CONUS). In an effort to develop a national flood forecasting system that was compatible with this modeling framework, the National Flood Interoperability Experiment [12,20] presented a method for computing the reach-average hydraulic property tables from a Height Above Nearest Drainage (HAND) raster [35,36]. Later, these tables were computed for each of the 2.7 million NHDPlusV2 reaches in CONUS [11,20] and a streamflow to depth relation was derived for depths, increasing at one-foot intervals from 0 to 82 feet. These tables are distributed as 1 CSV file per hydrologic unit (n = 331) totaling 33.1 GB of data. The process also computed auxiliary channel parameters like average Top Width and Bed Area. However, since these are based on the flooded extent as the rating curve is constructed, it includes overbank and basin averaged values and is not strictly a channel relation; their validity for hydraulic estimation is subject of future studies.

In 2018, [11] demonstrated a CyberGIS framework using 15 nodes of the ROGER hybrid supercomputing architecture to provide a proof of concept for inundation forecasts using the short-range NOAA National Water Model (NWM) forecast (at the time, a 15 hour time horizon). In that experiment, the national streamflow to depth conversion using the CFIM Hydro Property tables required 10 minutes (25% of the 40 total needed minutes), highlighting the computational demands at large scales even in High Performance Computing environments. In this research we extracted the requisite data from the hydrogeo-fulltable-${HUCID}.csv Property tables for version 2.1 [37].

2.2. Methods

2.2.1. Single Relation Curve Fitting

Preprints (www.preprints.org) | NOT PEER-REVIEWED | Posted: 21 December 2022 doi:10.20944/preprints202212.0390.v1

Power-law based rating curves fit the nonlinear form $Z = aQ^b$. When fitting a nonlinear curve to a set of data, the options are: (1) linearize the relationship by transforming the data; (2) fit a polynomial spline to the data; or (3) fit a nonlinear function. With our emphasis on interoperable power law relations, only the linear (1) and nonlinear (3) approaches are appropriate. Ordinary Least Squares (OLS) regression provides an analytical solution for minimizing the residual errors between the predicted and input data. It does this using a linear best fit with no iterative refinement. AHG relations are historically derived using OLS on the logarithmic transformation of the variables, where the exponential of the intercept provides the power law coefficient, and the slope of the linear model provides the power-law exponent. Several studies have highlighted the potential problem of using this approach [38] given that when the log transformed values are back-transformed, the estimates are effectively medians, and not means of the estimates, resulting in a general low bias [4].

Nonlinear Least Square (NLS) regression provides more flexible curve fitting through an iterative optimization. NLS approaches require a specified starting value for each unknown parameter to ensure the solver converges on a global rather than a local minimum. When suboptimal starting values are provided, NLS solvers may converge on a local minimum, or, not at all.

2.2.2. Curve Comparison Metrics

Part of our aim in this research is to evaluate how different curve fitting methods apply to "at-a-feature" hydraulic geometries (FHG) relations. To evaluate how well a given power law representation performs, a coefficient and exponent can be used to generate a set of predicted Z values (Z_p) for known Q values. The Root Mean Square Error (RMSE) between the observed (Z_o) and predicted Z values can then be computed and normalized by the mean of Z_o (nRMSE):

$$Z_{nRMSE} = 100 \times \frac{\sqrt{(z_0 - z_p)^2}}{\bar{z_0}} \quad (8)$$

The nRMSE metric was selected as it produces a unit of error with respect to a percentage and not the units of measurements, an important consideration when comparing error across measurements of depth (m), velocity (m/s), and top width (m), and across sites with variations in values that span several orders of magnitude. The Mean Absolute Percent Error (MAPE, equation 9) and percent bias, (Pbais, equation 10) are also computed.

$$Z_{mape} = \frac{100}{n} \times \sum \left| \frac{z_0 - z_p}{z_0} \right| \quad (9)$$

$$Z_{nRMSE} = 100 \times \frac{\sum z_p - z_o}{\sum z_o} \quad (10)$$

2.2.3. System-based Curve Fitting

Both OLS and NLS fit relationships by minimizing the error between the predicted and observed values. By solving each relationship independently, flow continuity (Equations 5-6) can be evaluated at the end, but only tells us if the system respects continuity or not. To solve the relationships as a system constrained by continuity, an algorithm needs to be able to minimize error in the face of multiple, potentially competing, objectives.

Evolutionary computing approaches (EA) provide stochastic search algorithms inspired by the principles of natural selection in which the "fittest" individuals from each

 doi:10.20944/preprints202212.0390.v1

population pass on their parameters to the next population, mimicking processes like selection, crossover, and mutation. The notion of "fittest" can be prescribed based on a user-defined objective function (OF).

When a time series for TW, U and Y are available, an objective function can be defined as the sum of each nRMSE (Equation 11) and solved with an elitist version of a Genetic Algorithm (GA) using the R package *GA* [39].

$$OF = \sum TW_{nRMSE}, U_{nRMSE}, Y_{nRMSE} \quad (11)$$

In the GA solver, solutions can be penalized for violating the continuity constraints by adding a weight to the resulting objective function. Using this type of objective function assumes the three nRMSE metrics are not competing, and that lowering, for example, TW nRMSE, will not increase nRMSE in the U or Y relation. To test whether fitting AHG is a multi-criterion optimization problem, the Non-dominated Sorting Genetic Algorithm II (NSGA-II) [40] elitist multi-objective Genetic Algorithm was implemented to minimize the Multi-Criterion OF (MCOF) defined in Equation 12, subject to the constraints shown in Equations 13,14.

$$MCOF = TW_{nRMSE}, U_{nRMSE}, Y_{nRMSE} \quad (12)$$

$$1 - allowance \leq b + f + m \quad (13)$$

$$1 - allowance \leq a \times c \times k \quad (14)$$

where the specified *allowance* variable represents the allowable deviation of perfect mass conservation allowed in the analytical solution.

NSGA-II is a multi-objective optimization algorithm with three key features including that it is elitist (the best solutions from each population carry on to the next); it uses an explicit diversity preserving mechanism based on crowing distance; and emphasizes non-dominated solutions in sorting. These mechanisms are controlled by defining the number of generations and populations, a crossover probability and distribution index, as well as a mutation probability and distribution index. More on these variables can be found in the original text of Deb et al, 2002. In the initialization and mutation of values, the algorithm expects an upper and lower bound of acceptable values for each unknown.

As a multi-objective solver, NSGA-II does not return a single answer but a Pareto front of "non-dominated" solutions. A non-dominated solution exists when none of the objective functions can be improved without degrading one of the others. Without additional, and often subjective preferencing, all Pareto optimal solutions are equally valid.

For hydraulic power law fitting, the multi-objective approach routinely provided more robust solutions from a global parameter set than a single objective GA algorithm suggesting there are competing objectives when minimizing error in the three relationships. While the GA could find solutions for many sites, it was never able to outperform the NSGA-II and required site specific parameter tuning and more generations to converge. The combinations of these factors gave us confidence in the multi objective approach.

2.2.4. Automated Workflow for Power Law Estimation and R Package Implementation

Figure 2 provides an outline for the automated workflow proposed for FHG estimation. To apply multiple techniques and increase the reproducibility of this research, an R package was written to implement this workflow [41]. The minimal requisite data needed are a series of flows (Q) and a corresponding hydraulic state (TW|U|Y). For each

Preprints (www.preprints.org) | NOT PEER-REVIEWED | Posted: 21 December 2022 doi:10.20944/preprints202212.0390.v1

provided state, a power law is fit using OLS and the solutions are used as starting values for an NLS solver. If only one or two hydraulic conditions are provided, continuity cannot be assessed, and results are returned. When three hydraulic states are provided, continuity is computed for the OLS and NLS solutions. If continuity for NLS or OLS is within a prescribed allowance (default = 0.05), the summary results are returned, and the solver concludes. If continuity is not met, the NSGA-II algorithm is run with 500 generations, a population size of 100, a crossover probability of 0.7, a crossover distribution index of 5, a mutation probability of 0.2, and a mutation distribution index of 10 using the *mco* R package [42]. These values were found after rigorous testing to balance solution skill and time to converge. For this application, the allowable lower and upper limits for the exponents (b,m,f) were set to {0,1}, and the coefficients (a,k,c) were limited to the range between 0 and the respective maximum found in the Afshari et al (2017) dataset + 20%. This last choice helped ensure the search space was adequate to find the best solutions while remaining realistic based on previous research in this domain.

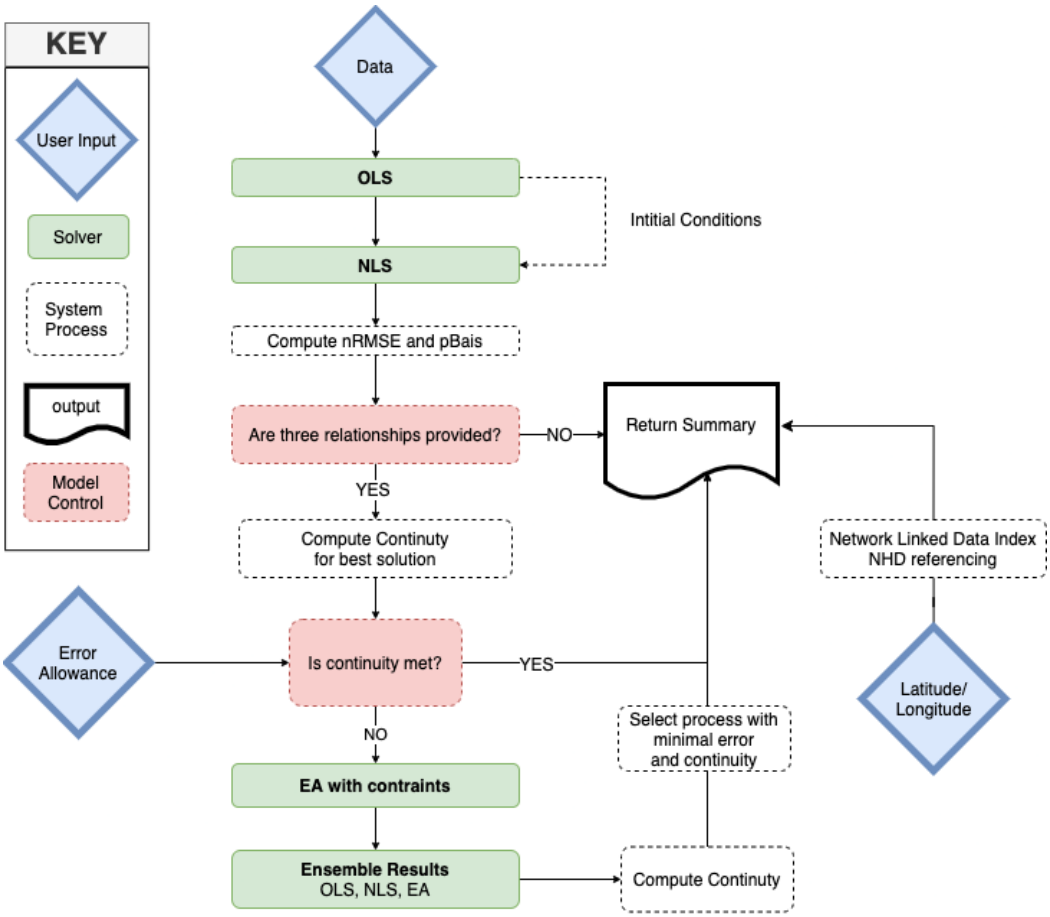

Figure 2. FHG optimization workflow based on user provided data.

Of the Pareto optimal solutions, the one yielding the minimum total nRMSE is selected and in cases where more than one solution have the same total error, the minimal sum of the absolute deviation from 1 in both continuity terms is selected.

In addition to the three "pure" options - OLS, NLS, and EA - a fourth "*Combination*" option is created by determining all possible exponent and coefficient combinations from the OLS, NLS, and EA solutions. For each of the 27 (i.e., $3^2 * 3$) options, the continuity constraints and nRMSE were computed and the solution producing the minimum total

Preprints (www.preprints.org) | NOT PEER-REVIEWED | Posted: 21 December 2022 doi:10.20944/preprints202212.0390.v1

error while preserving continuity was determined. If no viable *Combination* solution performs better than a "*pure*" solution, then no *Combination* set is returned.

Lastly, if a X and Y location are provided, the NHDPlus COMID (for locations in the USA) is appended to the summary output as a hydrologic address using the USGS Network Linked Data Index API in the *dataRetrival* Package. Toolsets like those found in the USGS HydroAdd [43], or nhdplusTools [44] can provide similar hydroaddressing capabilities for non NHDPlusV2 hydrofabrics.

3.5 Measuring Spatial Autocorrelation

Spatial autocorrelation is a measure of similarity between nearby observations [45]. A commonly used statistic to describe spatial autocorrelation is Moran's I which is a correlation coefficient multiplied by a spatial weights matrix [46,47]. In this research the weights matrix is computed as the inverse distance (1/distance) between two locations. The Moran's I test requires non-skewed data, therefore in all applications of Moran's I in the research, skewness was evaluated, and, when needed, data was transformed (by square root or logarithmically) and tested to ensure minimal skewness.

The expected value of Moran's I under the null hypothesis of no spatial autocorrelation is equal to -1/(N-1), where N represents the sample size. Values significantly below this indicate negative spatial autocorrelation meaning values are dissimilar from their neighbors. Values significantly greater than -1/(N-1) indicate positive spatial autocorrelation. To test for statistical significance, we use a Monte Carlo simulation where values are randomly assigned to each of N points, and the Moran's I is computed. This is repeated over a set number of repetitions to establish an expected distribution. The Moran's I computed on the observed data is then compared with the distribution to see how likely the observed values could be random.

3. Results

The automated workflow discussed in the methods section was implemented for all USGS and CFIM rating curves as well as the HYDRoSWOT dataset.

3.1. Single Relation Curve Fitting (Rating Curve Estimation)

Figure 3 shows the results of the OLS and NLS power law fitting methods for the USGS and CFIM rating curves. Row one (panels a-c) shows three illustrative examples of how each method was able to reproduce the USGS rating curves. The sites shown are those with an OLS nRMSE closest to the 25th, 50th, and 75th percentile of the dataset. In all images, black curves represent the true rating relationship, red curves represent the NLS fit, and the blue curves represent the OLS fit.

At the 25th percentile, both methods replicate the USGS rating curve within ~1% error. The NLS approach has a slightly lower nRMSE and both methods slightly underpredict at the top end of the curve. At the 50th and 75th percentile, the underprediction at the top of the curve becomes more prominent, but NLS solutions better capture the shape of the observations with half to a third amount of error. To express these errors across the entire dataset, the cumulative distribution of the Mean Absolute Percent Error (MAPE), percent bias, and nRMSE are shown in row 2 (panels d-f). The most distinct difference between fitting methods is evident in the nRMSE and percent bias with less error and bias evident in the NLS solutions.

Row 3 (panels g-i) shows three illustrative examples, selected in the same way as row 1, from the CFIM dataset. Here, OLS tends to overpredict at the higher flow records. CFIM SRC's tend to conform more closely to true power law shape, in part because the process used to generate them populated Manning's equation which takes a power law form. As a result, even at the 75th percentile error, the error exhibited is less than the 25th percentile error in the observed USGS rating curves. However, NLS solutions still have >3 times less error than the OLS solutions past the 50th percentile.

Preprints (www.preprints.org) | NOT PEER-REVIEWED | Posted: 21 December 2022 doi:10.20944/preprints202212.0390.v1

The final row (panels j-l) shows the cumulative error distributions for all 2.6 million CFIM rating curves. The same pattern as seen in row 2 emerges in that NLS can reduce error and bias across the collection of relationships when compared to OLS. Overall, these results confirm our expectation that an NLS fit, starting with the values found with OLS, can reduce the overall error in the solution.

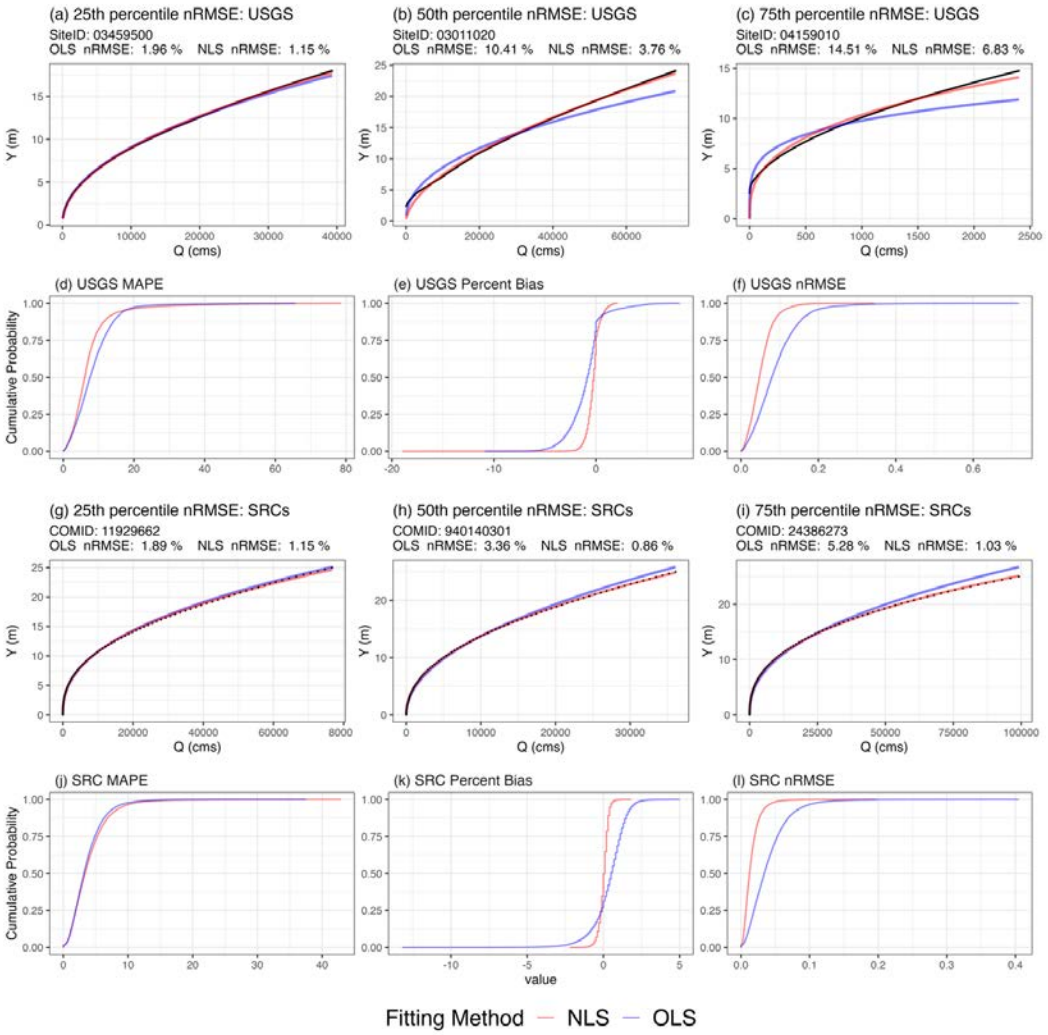

Figure 3. Panel (a-c) shows three illustrative sites approximating the 25th, 50th and 75th percentile nRMSE error for the OLS methods produced across the USGS sites. Panel (d-f) shows the empirical cumulative distribution function (ECDF) for MAPE, Pbais, and nRMSE across all tested sites using the OLS and NLS method. Panel (g-i) show three illustrative sites approximating the 25th, 50th and 75th percentile nRMSE error for the OLS methods produced across the SRC sites. Panel (j-i) shows the ECDF curve for MAPE, Pbais, and nRMSE across all tested sites using the OLS and NLS method.

3.2. System-based Curve Fitting Methods

Next, we explore the error in solutions that fit all three relationships. Figure 4 shows the results of the OLS, NLS, EA, and Combination fits across the HYDRoSWOT dataset. Panel (a) shows the distribution of errors for each method across the three hydraulic relationships as well as the total system error. The overall error distributions are shown as violin plots with the mean error marked as a black dot in each method/relation pair. At the top of each boxplot the mean error for each relationship is ranked - with 1 being the lowest error. Here it becomes evident that - across relationships - the Combination approach produces the lowest mean error, NLS produces the second lowest, and except for Top Width OLS produces the third lowest while EA generates the largest mean error. This

Preprints (www.preprints.org) | NOT PEER-REVIEWED | Posted: 21 December 2022 doi:10.20944/preprints202212.0390.v1

provides evidence that the final Combination step is indeed able to find solutions with less error than any single method approach.

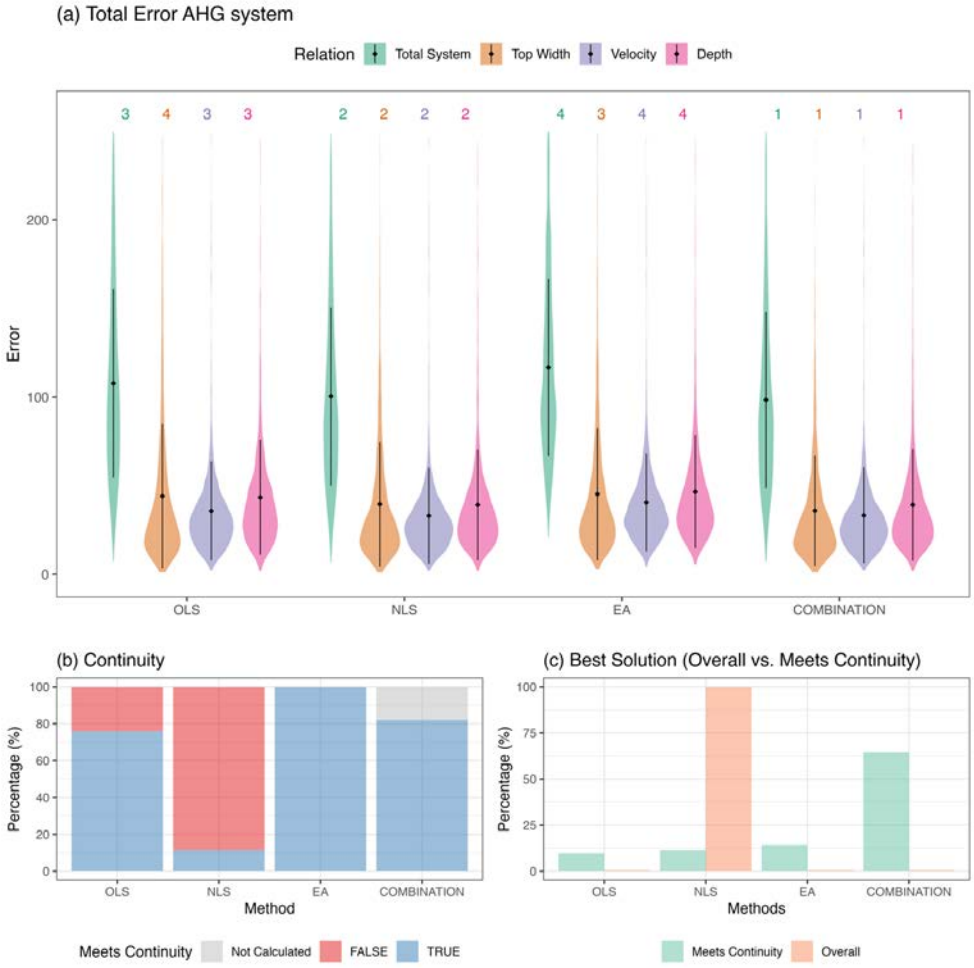

Figure 4. Summary of the FHG optimization over USGS field sites. (a) Violin plots of error between observed records and FHG estimates using different fitting techniques. (b) The percent of sites where each method yielded FHG parameters that met continuity. (c) The percent of sites where each method yielded the minimal total error.

Panel (b) shows the percentage of solutions in each method that meet continuity. In ~25% of the cases OLS fails to find a valid solution whereas NLS fails in almost 85% of the time. By design, the EA approach is always able to find a valid solution and the Combination approach - when calculated - does as well.

Panel (c) shows the percentage of relations that were best fit by each method regardless of continuity and those that provided the best mass conserving fit (e.g., were physically valid). The sequence of fitting is OLS → NLS → EA → Combination, therefore, if a solution is found earlier in the sequence, it counts towards that method, for example if OLS and NLS provide the same solution, OLS is given credit as the best fitting method. Looking first at the green bars, when continuity is ignored, NLS finds the best solution in 100% of the cases, a finding that is consistent with section 4.1.

Again, NLS proves to be the best approach for finding minimal error in cases where continuity cannot be enforced, however minimizing the error in each relationship independently yields results that 9/10 times violate continuity (see panel(b)). The fact that NLS finds better individual relations that in turn violate continuity, confirms that solving AHG relations to enforce continuity is a multi-criterion problem.

 doi:10.20944/preprints202212.0390.v1

Looking at the purple bars, the standard OLS approach is only able to find the best viable solution in ~7% of the locations. Given it is the de facto standard, this is a critical finding. Alternatively, the evolutionary NSGA–II approach - as expected - can always find physically valid solutions along a Pareto front, however, results in increased error.

The Combination approach, which acts as a final permutation on the possible set of coefficients and exponents in the EA solution, routinely can utilize the OLS, NLS and EA solutions to provide a mass conserving solution that also yields minimal error. This highlights that when physical validity is of concern, the ability for the *Combination* approach to use information from all three methods to identify the optimal AHG system is important.

The key takeaway is that NLS can best fit individual power-laws but in the face of MCOP - of which AHG problems are - TW, U and Y become competing objectives. Using multi-criterion EA as the sole fitting function ensures continuity is preserved and yields a Pareto front of possible solutions. However, it is the combination of all three fitting methods which produces the most optimal solution, balancing the strengths of solving the equations individually and as a system.

3.3. OLS vs Statistical Data Filtering vs FHG fitting

Solution error and flow discontinuity in AHG/FHG relationships stem from noise in the observation data either from errors in measurement, or changes to the river system over time. To date, Afshari et al, (2017) is the only research that has looked at ways to reduce noise in anticipation of fitting many hundreds, if not thousands of relations. They proposed a statistical pre-processing [1] that - much like OLS/NLS - is applied to each relationship independently prior to OLS fitting. Given we understand fitting the AHG system to be a MCOP, we want to compare the results found with each method across the HYDRoSWOT dataset. To do so, the reported streamflow from the HYDRoSWOT measurements were used to compute nRMSE for TW, Y and U using the AHG/FHG variables produced here and in [48,49].

In the top row of figure 5, the continuity violations for the exponents, coefficients and total system are shown for each method. In the bottom row of figure 5, the error distributions for each relation/method are shown again with the ranked mean error by relation shown in the top.

The traditional OLS method can provide relatively minimal error but 25% of the locations do not achieve flow continuity. The statistical filtering method based on an allowable range of 0.95-1.05 does worse than OLS with respect to continuity and overall error. The FHG workflow achieves lower error distributions than those produced using the OLS method, while ensuring mass is preserved at each site. Thus, from the standpoint of the metrics tested, the FHG method is better suited to consume raw data and produce physically viable solutions with minimal error the advanced fitting (NLS) or statistical preprocessing. This is advantageous as the methods can be applied to any set of data and do not require a priori preprocessing or filtering.

Preprints (www.preprints.org) | NOT PEER-REVIEWED | Posted: 21 December 2022 doi:10.20944/preprints202212.0390.v1

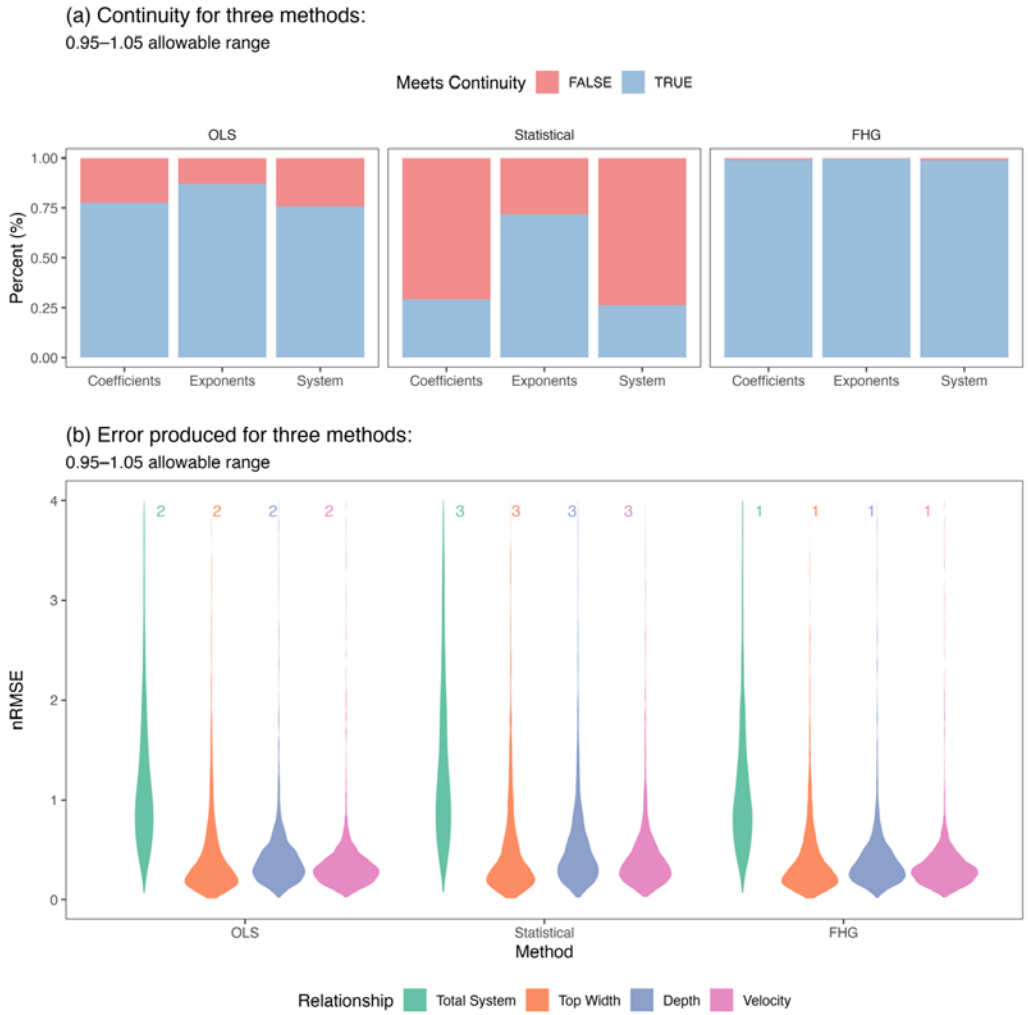

Figure 5. Panel (a) shows the continuity violations for the exponents, coefficients, and total system for each method. In Panel (b) the error distributions for each relation grouped by method are shown with the ranked mean error by relation shown in the top.

3.4. Data Reduction, Extensibility, and Spatial Correlation

One challenge with a large set of rating tables is the size of data files and the ease of application. With respect to data reduction, the USGS rating curves are reduced from 44,838,260 values to 15,064 values (0.03% of their original size) with the median cost of 1.6% nRMSE. Equally, the SRCs are reduced from 128,475,500 values to 5,139,020 values (4% of their original size) with a median cost of 0.5% nRMSE. This highlights the computational efficiency of this approach with a minimal loss in accuracy. The outstanding challenge is how these reduced datasets can benefit ungauged site prediction.

Different studies through time have tried to map AHG relations at various scales [8,18,50] and recent studies have utilized small to moderate sets of river surveyed data in search of generalizable patterns (described well in [1]).To date though a limited set of general patterns have been identified using statistical relationships between geomorphic, geographic, or hydrographic properties. Being able to estimate AHG parameters in ungauged locations is a problem well suited to data-driven approaches (e.g. “machine learning”) that generally require (1) a set of learnable values and (2) a large set of training data associated with a rich set of predictor variables.

 doi:10.20944/preprints202212.0390.v1

Reducing the hydraulic representation to the set of {a,b,c,k,f,m} values provides a concise form of interrelated parameters that are well suited for training. The simplicity of these relations allows for the training and discovery of more flexible classification and predictive models. Further, the laws of continuity not only provide a constraint, but a way to infer missing data meaning two of the three relationships needs to be known.

Hydroaddressing to a national dataset like the NHDPlusV2 provides the ability to associate rich sets of predictor variables that are related to not only the incremental features but can be accumulated along the hydrologic network. Ongoing federal efforts at the USGS and NOAA are working to collaboratively build an authoritative reference hydrofabric [28] from which application ready data products [26] can be built for needs including but not limited to the NOAA Next Generation Water Modeling Framework [29], its anticipated implementation as version 4 of the National Water Model, and the USGS National Hydrologic Model [51]. The reference fabric includes a robust and well tested set of flowpath network properties (e.g., pathlength, order, arbolate sum) and set of catchment-based meteorologic, geographic, and geomorphological characteristics (e.g., mean aridity, average clay content).

Many data driven approaches are sensitive to spatial autocorrelation (neighbors affecting neighbors) which can influence model choice and fitting routines. Moran's I is a measure of spatial autocorrelation, however the Moran's I statistic is not robust to outliers or strongly skewed datasets. When accessed it was found that the coefficients (a, c, k) were strongly skewed but could be normalized with a log transformation. To quantify the amount of spatial autocorrelation across the FHG parameters, and total system error, the Moran's I and its statistical significance were calculated over 999 Monte Carlo simulations. The results of these are shown in Figure 6.

The curve in each plot shows the distribution of Moran I values we would expect had the input values been randomly distributed across the FHG locations. In all cases the observed statistic falls well to the right of the distribution indicating clustering (positive correlation) in each of the coefficients, exponents, and system error. The P-value of .001 in all cases provides evidence that this clustering is statistically significant.

Not only do the AHG parameters display spatial autocorrelation, but so do the total error measures. This could be due to rivers in the area changing more rapidly in time, difficulty in measuring, changes in measuring crews, or it could point back to Ferguson's

4. Discussion

While the results section focused on the numerical improvements the FHG fitting method offers in the face of noisy observation data, the discussion aims to highlight the computational advantages of having these relations documented as a set of lightweight features. We do this looking specifically at three areas of (1) data interoperability (2) multiscale application (3) probabilistic representation.

4.1. Interoperability and Comparison

One motivation for pursuing the FHG relations was the potential for greater interoperability between systems. This need is exemplified in the following set of tasks: To compare a USGS rating curve to a CFIM SRC or replace the CFIM SRC with the USGS rating curve in the continental dataset. As it stands, both would be challenging using tabular representations. Figure 7 shows a high-level comparison made possible by power law forms and plots the differences in coefficients and exponents for both the OLS and NLS fits as [SRC_x - USGS_x]. By subtracting the USGS values from the repressive SRC values, negative values indicate that the SRCs are underpredicting, while positive values imply the opposite.

In Figure 7, panel (a) shows the coefficient comparison [SRC - USGS] for the OLS and NLS fits. The red box outlines the amount and predominant direction of over or under prediction in each value/fitting method while the green boxes outline the amount of data

Preprints (www.preprints.org) | NOT PEER-REVIEWED | Posted: 21 December 2022 doi:10.20944/preprints202212.0390.v1

points within +- 10% of each other. Here The CFIM rating curves tend to overpredict the coefficient value which is exacerbated in the OLS relationships. Panel (b) shows the exponent comparison [SRC - USGS] and that the CFIM rating curves tend to underpredict the exponent value. This underprediction is also exacerbated in the OLS relationships.

Overall, this comparison provides some direct insight into the trends of the SRCs - specifically that they tend to underestimate the value of *f*, while overestimating the value of *c*. In panel (c), a conceptual rating curve is shown in black in which +-10% is added/subtracted from c and f. We see the implications of poorly fitting f are larger than c and combined the systematic underprediction of *f* and over prediction of *c* leads to CFIM-SRCs that tends to underpredict. This is exacerbated in the OLS fitting and is supported by the descriptions in Dingman & Afshari (2018) that OLS results in a general low bias.

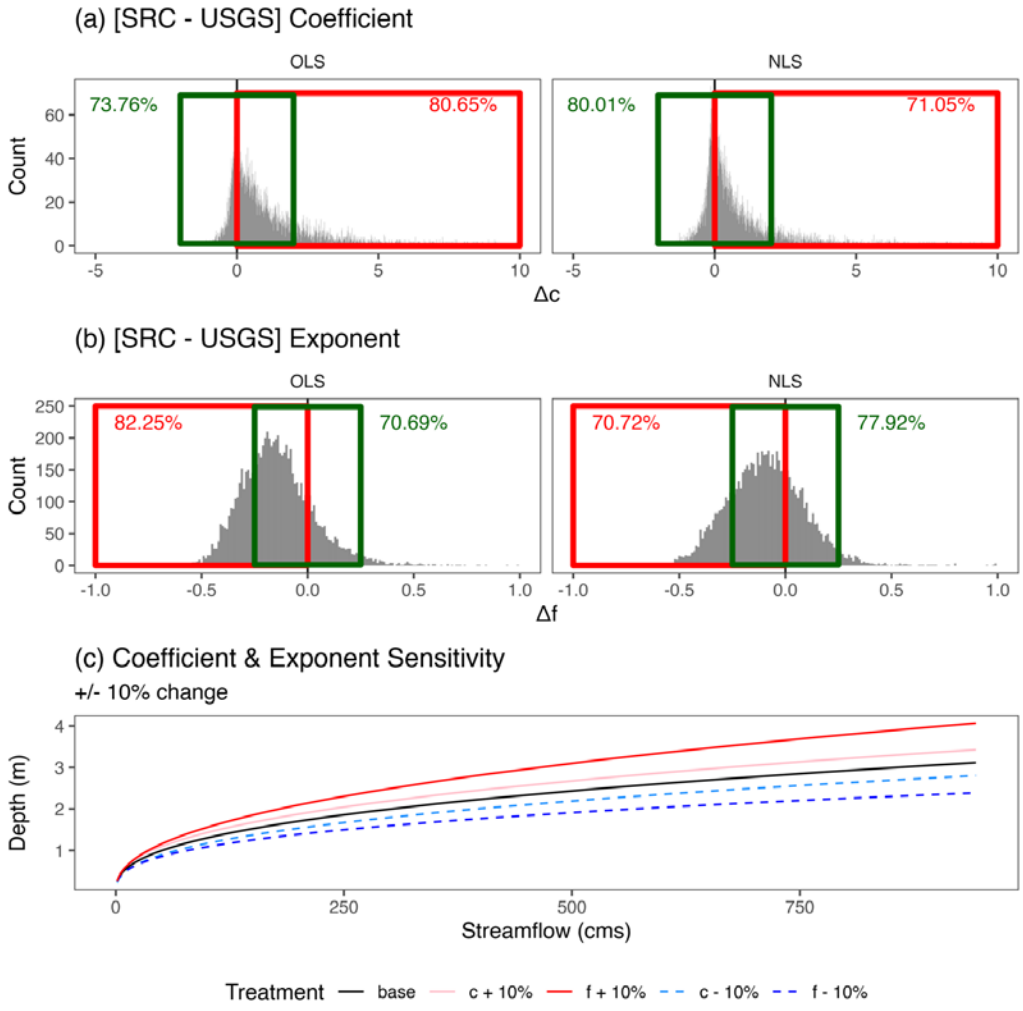

Figure 7. FHG relations make rating curves from different systems, table schemas, and methods directly comparable at the individual locations and across larger domains. Panel (a) highlights the comparisons of the USGS and SRC coefficients as [SRC - USGS]. The red box outlines the amount and predominant direction of over or under prediction in each value/fitting method while the green boxes outline the amount of data points within +- 10%. Panel (b) highlights the comparisons of the USGS and SRC exponents as [SRC - USGS]. Panel (c) shows a conceptual rating curve in black in which +-10% is added/subtracted from the c and f to visualize the magnitudes of these error.

4.2. Reach to continental scale flood forecasting

Preprints (www.preprints.org) | NOT PEER-REVIEWED | Posted: 21 December 2022 doi:10.20944/preprints202212.0390.v1

Reducing the CFIM SRCs to power-law relations simplifies the continental flood mapping workflow while making SRCs more accessible. All hydroaddressed CFIM-FHG relations can be stored in a NetCDF file that is 0.01% of the original 33 GB CSVs. To enhance mapping, access, and subsetting capabilities, latitude and longitude can be added increasing the file size to 0.06% of the original data. Using this new approach, the time needed to produce a national depth file for an NWM forecast/hindcast takes less than 2 seconds on a personal laptop. While this does not solve the depth to extent steps, the performance gain would save 25% of the time currently needed on the HPC cluster for real-time flood prediction.

To illustrate this process, Figure 8 highlights the code for downloading a National Water Model channel output file from the reanalysis simulation and using the local FHG file to generate a spatially referenced depth forecast for August 27, 2017, at 12:00 UTC (landfall of Hurricane Harvey). To provide a visual assessment, we mapped the locations with the top 1% flows in the country and juxtaposed it with a remotely sensed flood map for the same date from the Dartmouth Flood Observatory [52]. Overall, the prediction shows the major river arteries exhibiting high depths, as well as a cluster along the southeastern coast of Texas near Houston that is aligned with the landfall of Hurricane Harvey and the remotely observed flood extents.

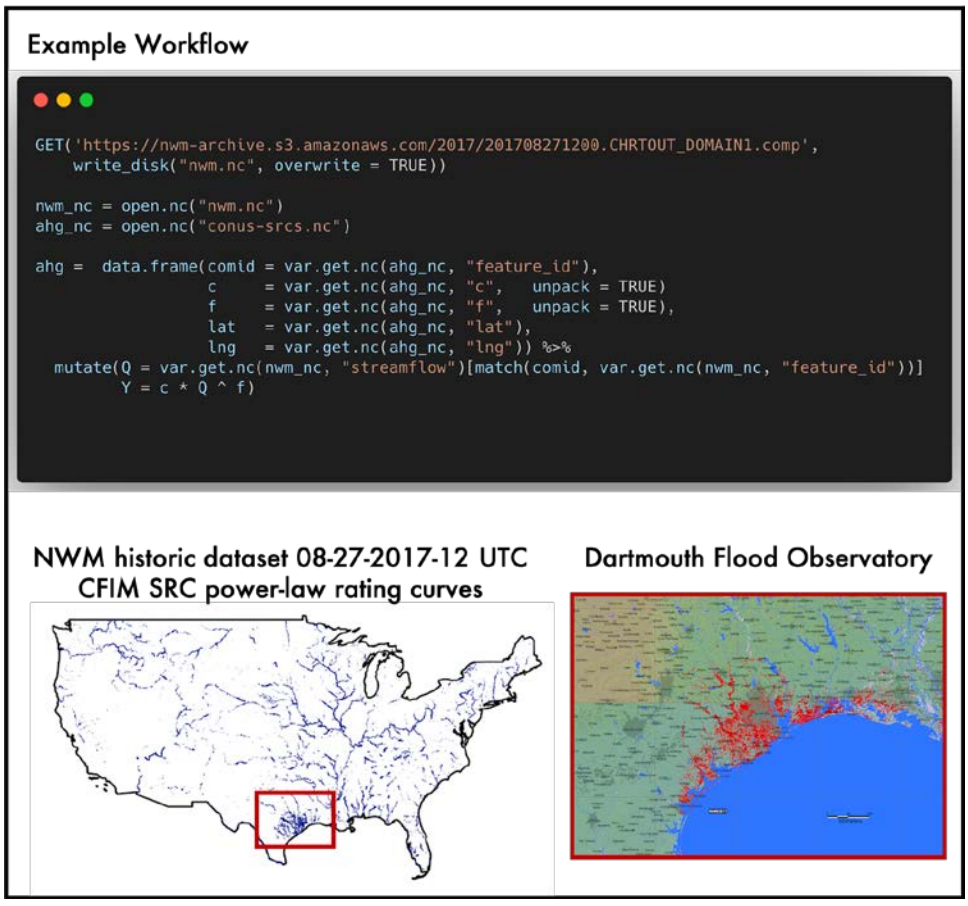

Figure 8. (A) example code for translating a channel output file for the National Water Model into a depth table with coordinates assuming the existence of a NetCDF with FHG term and addresses. Including data download, this process required 2.78 seconds to execute. The lower left-hand map shows the top 1% of depths produced in the red box highlights the area surrounding the landfall of Hurricane Harvey. In the lower right, the flood extents from August 27th, 2017, as observed by Brakenridge (2022) show clear correlation with the FHG high flows.

Other studies have evaluated the skill of SRCs [53,54] and compared simulated inundation to remotely sensed flood maps and aerial imagery [13,55] but such analyses are

 doi:10.20944/preprints202212.0390.v1

beyond the scope of the illustrative use case here which simply focuses on the methods efficiency.

4.3. Probabilistic Evaluation and Data Fusion

It is well documented that rating curves are inherently uncertain [15]. These uncertainties become even more prevalent in synthetic systems (e.g., CFIM) and in remote sensing practices like flood water classification, top width extraction, and velocimetry measurements. With tabular forms of data, there is no clear way to represent multiple possible relations for a given location easily.

Additionally, there is no straightforward path for integrating multiple rating curve representations in a computation workflow. Returning to flood mapping via DEM derived SRCs and the HAND method there are two prominent issues that have been recognized to date. These include a "cross boundary" issue and a "global roughness" issue. For the former, DEMs cells are considered flooded if and only if the normalized elevation of that cell is less than depth of water associated with the "nearest drainage" SRC. However, many locations on the landscape can flood from more than their nearest drainage. When the conceptual model does not allow this to happen, artificial "walls" of water can pile up at catchment boundaries. The capacity for multiple river segments to contribute to a single cell is being evaluated in NOAA-OWP FIM4 using the "Generalized Mainstems" model. While this advances the conceptual model, it results in having upwards of 20 possible SRCs needing to be evaluated for a given cell to be evaluated. For the second issue, the use of global or stream order-based roughness values has proven insufficient for estimating accurate SRCs.

The ability to compute and represent multiple rating curves for a single feature provides the pathway towards probabilistic rating curves. In the case of SRCs, following the approach highlighted here it is possible for 100 rating curves to be generated with slight variations in roughness - or a collection of Generalized Mainstem SRCs to impact a given location. In doing this and calculating depths across all hundred options provides the capability to compute and communicate uncertainty in the generated forecasts more adequately.

To illustrate this, Figure 9 shows a JavaScript Object Notation (JSON) representation of four rating curves at a specific NWIS site in panel (a). In the JSON, there is a siteID and COMID property and a list of plausible rating relationships at this site. A daily streamflow series was downloaded from NWIS, using the NWIS site ID, and from it, a depth time series was generated with the respective USGS and CFIM NLS and OLS fits. The black line shows a pseudo ensemble of these four rating curves computed from the generated depth series, and the orange line shows the results of using the 1,048 row USGS rating curve as a lookup table from which the closest value is extracted and the minimum depth in the table is subtracted to adjust to the reference datum.

The USGS-NLS and ensemble depth series can capture the signal in the lookup series well. Notably, both SRC representations are lower than the expected, but the NLS approach is a closer representation. The under prediction is potentially indicative of the pattern seen in Figure 9, that the SRC formulation tends to underpredict the coefficient of the respective rating curves. Interestingly the USGS OLS fit is arguably the worst over predicting depths across the timeseries. Again, the expected series is simply an estimate due to the unknown reference and this example is meant to illustrate the opportunity to use FHG representations to extend the utility and interoperability of disparate systems to expedite computation and better capture variability in a highly uncertain phenomenon.

Preprints (www.preprints.org) | NOT PEER-REVIEWED | Posted: 21 December 2022 doi:10.20944/preprints202212.0390.v1

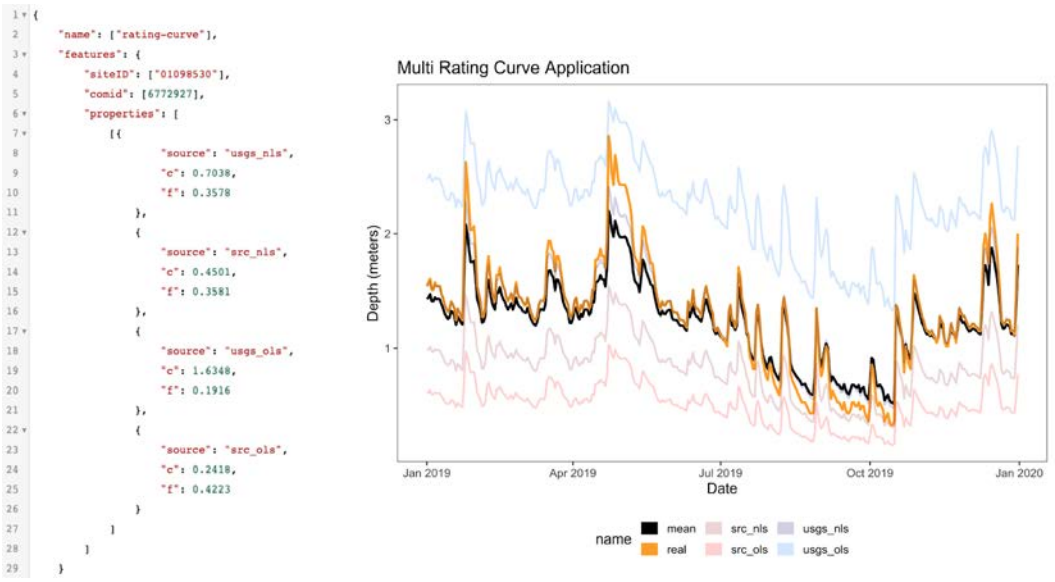

Figure 9. Multiple representations of a rating curve can be stored as a JSON object. Parsing such a file can generate many possible depths time-series that can be used individually, or as an ensemble (here we show a basic mean in black). For verification, we overlay the rating curve computed from the USGS rating curve table available on NWIS (orange) where depths are corrected by subtracted the minimum record.

5. Conclusions

Rating relationships of often noisy river survey and discharge data are typically stored in tabular form and distributed site-by-site or as massive tables of data. The ability to reduce these tabular representations to power law relations is useful for data access, application, and integration. The use of power-law models are well established approximations for at-a-station hydraulic relationships, but the parameterization of these models requires non-trivial analysis. In this paper we focus on the representation of hydraulic relationships for the purpose of efficient data exchange and application in modeling systems that require the use of many locations or the integration of multiple datasets. We present a sequential fitting method that uses OLS, NLS, and MCOP curve fitting methods to reduce error and ensure physically valid solutions. This process is efficient, reproducible, and publicly available as an R package. With this tool, we fit AHG relations to the entirety of the USGS Rating Curve database, the entirety of the USGS HYDRoSWOT data (with at least 30 years of record), and the 2.7 million hydraulic property tables produced as part of the CFIM.

For single relationships, the NLS method always produces better fitting ratings than OLS alone. When TW, Y and U relationships are known it becomes evident that NLS fits routinely yield relationships that violate continuity, suggesting that minimizing system error in each relationship represents a competing objective. To resolve this, a common, well studied, multi-objective evolutionary algorithm was used to produce a Pareto Front solution with minimal error. Equally important, the algorithm allows for the physical constraints of continuity/mass conservation to be enforced in the solution. The advantages of this approach were illustrated by the volume of data reduction (99.7%), the capacity for increased interoperability, and the speed at which it supports the exchange of streamflow data to other hydraulic states at a continental scale. Equally important, the focus on representation provides the opportunity for supporting probabilistic and multi realizations of the rating process indexed by hydrologic address. Future work can focus on using these relationships to predict AHG relations in rivers with limited to no survey data to improve our understanding of these processes, and to support large-scale modeling, measurement, and evaluation efforts through better representation, addressing, and multi-realization approaches.

Author Contributions: Conceptualization, J Michael Johnson and Shahab Afshari; Data curation, J Michael Johnson; Formal analysis, J Michael Johnson; Funding acquisition, Keith Clarke and Lilit Yeghiazarian; Methodology, J Michael Johnson, James Coll, Keith Clarke and Shahab Afshari; Software, J Michael Johnson; Validation, J Michael Johnson and James Coll; Writing – original draft, J Michael Johnson; Writing – review & editing, J Michael Johnson, James Coll, Keith Clarke, Shahab Afshari and Siddharth Saksena. Funding: This work was partially supported with funding from the National Science Foundation's (Grants 1937099, 2033607). Any opinions, findings, and conclusions or recommendations expressed in this material are those of the authors and do not reflect the views of the National Science Foundation.

Funding: This work was partially supported with funding from the National Science Foundation's (Grants 1937099, 2033607). Any opinions, findings, and conclusions or recommendations expressed in this material are those of the authors and do not reflect the views of the National Science Foundation.

Data Availability Statement: Data used in the study can be accessed at the following locations. The CFIM data was accessed from (Liu et al., 2020). USGS Ratings Curves were accessed for all feasible gauge IDs using the *dataRetrival* R package [34]. USGS field measurements were downloaded from the USGS HYDRoacoustic dataset in support of the Surface Water Oceanographic Topography satellite mission (HYDRoSWOT) data release [23]. All FHG curves were fitted using the AHGestimation software [41].

Conflicts of Interest: The authors declare no conflict of interest.

References

1. Afshari, S.; Fekete, B.M.; Dingman, S.L.; Devineni, N.; Bjerklie, D.M.; Khanbilvardi, R.M. Statistical Filtering of River Survey and Streamflow Data for Improving At-a-Station Hydraulic Geometry Relations. *Journal of Hydrology* **2017**, *547*, 443–454.
2. Leopold, L.B.; Maddock, T. *The Hydraulic Geometry of Stream Channels and Some Physiographic Implications*; US Government Printing Office, 1953; Vol. 252;.
3. Dingman, S.L. Analytical Derivation of At-a-Station Hydraulic–Geometry Relations. *Journal of Hydrology* **2007**, *334*, 17–27.
4. Dingman, S.L.; Afshari, S. Field Verification of Analytical At-a-Station Hydraulic-Geometry Relations. *Journal of Hydrology* **2018**, *564*, 859–872.
5. Orlandini, S.; Rosso, R. Parameterization of Stream Channel Geometry in the Distributed Modeling of Catchment Dynamics. *Water Resources Research* **1998**, *34*, 1971–1985.
6. Western, A.W.; Finlayson, B.L.; McMahon, T.A.; O'Neill, I.C. A Method for Characterising Longitudinal Irregularity in River Channels. *Geomorphology* **1997**, *21*, 39–51.
7. Jowett, I. Hydraulic Geometry of New Zealand Rivers and Its Use as a Preliminary Method of Habitat Assessment. *Regulated Rivers: Research & Management: An International Journal Devoted to River Research and Management* **1998**, *14*, 451–466.
8. Andreadis, K.; Brinkerhoff, C.; Gleason, C. Constraining the Assimilation of SWOT Observations with Hydraulic Geometry Relations. *Water Resources Research* **2020**, *56*, e2019WR026611.
9. Gleason, C.J.; Smith, L.C. Toward Global Mapping of River Discharge Using Satellite Images and At-Many-Stations Hydraulic Geometry. *Proceedings of the National Academy of Sciences* **2014**, *111*, 4788–4791.
10. Johnson, J.M.; Narock, T.; Singh-Mohudpur, J.; Fils, D.; Clarke, K.C.; Saksena, S.; Shepherd, A.; Arumugam, S.; Yeghiazarian, L. Knowledge Graphs to Support Real-time Flood Impact Evaluation. *AI Magazine* **2022**, *43*, 40–45, doi:10.1002/aaai.12035.
11. Liu, Y.Y.; Maidment, D.R.; Tarboton, D.G.; Zheng, X.; Wang, S. A CyberGIS Integration and Computation Framework for High-Resolution Continental-Scale Flood Inundation Mapping. *Journal of the American Water Resources Association* **2018**.
12. Maidment, D.R. Conceptual Framework for the National Flood Interoperability Experiment. *JAWRA Journal of the American Water Resources Association* **2016**, *53*, 245–257.
13. Johnson, J.M.; Munasinghe, D.; Eyelade, D.; Cohen, S. An Integrated Evaluation of the National Water Model (NWM)–Height Above Nearest Drainage (HAND) Flood Mapping Methodology. *Natural Hazards and Earth System Sciences* **2019**, *19*, 2405–2420.

14. Brackins, J.; Moragoda, N.; Rahman, A.; Cohen, S.; Lowry, C. The Role of Realistic Channel Geometry Representation in Hydrological Model Predictions. *JAWRA Journal of the American Water Resources Association* **2021**, *57*, 222–240.
15. McMillan, H.; Westerberg, I. Rating Curve Estimation under Epistemic Uncertainty. *Hydrological Processes* **2015**, *29*, 1873–1882.
16. USGS FAQ, M. and A.W. How Is a Rating Curve Used to Convert Gage Height into Streamflow? | U.S. Geological Survey Available online: https://www.usgs.gov/faqs/how-rating-curve-used-convert-gage-height-streamflow (accessed on 29 September 2022).
17. Lin, P.; Pan, M.; Allen, G.H.; de Frasson, R.P.; Zeng, Z.; Yamazaki, D.; Wood, E.F. Global Estimates of Reach-level Bankfull River Width Leveraging Big Data Geospatial Analysis. *Geophysical Research Letters* **2020**, *47*, e2019GL086405.
18. Yamazaki, D.; O'Loughlin, F.; Trigg, M.A.; Miller, Z.F.; Pavelsky, T.M.; Bates, P.D. Development of the Global Width Database for Large Rivers. *Water Resources Research* **2014**, *50*, 3467–3480.
19. Yang, X.; Pavelsky, T.M.; Allen, G.H.; Donchyts, G. RivWidthCloud: An Automated Google Earth Engine Algorithm for River Width Extraction from Remotely Sensed Imagery. *IEEE Geoscience and Remote Sensing Letters* **2019**, *17*, 217–221.
20. Zheng, X.; Tarboton, D.G.; Maidment, D.R.; Liu, Y.Y.; Passalacqua, P. River Channel Geometry and Rating Curve Estimation Using Height above the Nearest Drainage. *Journal of the American Water Resources Association* **2017**.
21. Armstrong, D.W.; Holnbeck, S.R.; Chase, K.J. *Evaluating the Use of Video Cameras to Estimate Bridge Scour Potential at Four Bridges in Southwestern Montana*; US Geological Survey, 2022;
22. Wood, E.F.; Ming, P. *Algorithm Development for SWOT River Discharge Retrievals*; NASA JPL, 2017;
23. Canova, M.G.; Fulton, J.W.; Bjerklie, D.M. USGS HYDRoacoustic Dataset in Support of the Surface Water Oceanographic Topography Satellite Mission (HYDRoSWOT) 2016.
24. Blodgett, D.; Johnson, J.M.; Sondheim, M.; Wieczorek, M.; Frazier, N. Mainstems: A Logical Data Model Implementing Mainstem and Drainage Basin Feature Types Based on WaterML2 Part 3: HY_Features Concepts. *Environmental Modelling & Software* **2020**, 104927.
25. Blodgett, D.; Dornblut, I. OGC WaterML 2: Part 3-Surface Hydrology Features (HY_Features)-Conceptual Model. Version 1.0. **2018**.
26. Blodgett, D.L.; Johnson, J.M. Hydrologic Modeling and River Corridor Applications of HY_Features Concepts. 2022.
27. McKay, L.; Bondelid, T.; Dewald, T.; Johnston, J.; Moore, R.; Rea, A. NHDPlus Version 2: User Guide. *US Environmental Protection Agency* **2012**.
28. Bock, A.; Blodgett, D.L.; Johnson, J.M.; Santiago, M.; Wieczorek, M.E. National Hydrologic Geospatial Fabric Reference and Derived Hydrofabrics 2022.
29. Johnson, J.M. National Hydrologic Geospatial Fabric (Hydrofabric) for the Next Generation (NextGen) Hydrologic Modeling Framework 2022.
30. Yamazaki, D.; Ikeshima, D.; Sosa, J.; Bates, P.D.; Allen, G.H.; Pavelsky, T.M. MERIT Hydro: A High-Resolution Global Hydrography Map Based on Latest Topography Dataset. *Water Resources Research* **2019**, *55*, 5053–5073, doi:10.1029/2019WR024873.
31. Dallo, I.; Stauffacher, M.; Marti, M. What Defines the Success of Maps and Additional Information on a Multi-Hazard Platform? *International Journal of Disaster Risk Reduction* **2020**, *49*, 101761.
32. Johnson, J.M.; Coll, J.M.; Ruess, P.J.; Hastings, J.T. Challenges and Opportunities for Creating Intelligent Hazard Alerts: The "FloodHippo" Prototype. *Journal of the American Water Resources Association* **2018**.
33. Kuller, M.; Schoenholzer, K.; Lienert, J. Creating Effective Flood Warnings: A Framework from a Critical Review. *Journal of Hydrology* **2021**, *602*, 126708.
34. De Cicco, L.A.; Lorenz, D.; Hirsch, R.M.; Watkins, W.; Johnson, M. *DataRetrieval: R Packages for Discovering and Retrieving Water Data Available from U.S. Federal Hydrologic Web Services*; U.S. Geological Survey / U.S. Geological Survey: Reston, VA, 2018;

35. Nobre, A.D.; Cuartas, L.A.; Hodnett, M.; Rennó, C.D.; Rodrigues, G.; Silveira, A.; Waterloo, M.; Saleska, S. Height Above the Nearest Drainage–a Hydrologically Relevant New Terrain Model. *Journal of Hydrology* **2011**, *404*, 13–29.
36. Rennó, C.D.; Nobre, A.D.; Cuartas, L.A.; Soares, J.V.; Hodnett, M.G.; Tomasella, J.; Waterloo, M.J. HAND, a New Terrain Descriptor Using SRTM-DEM: Mapping Terra-Firme Rainforest Environments in Amazonia. *Remote Sensing of Environment* **2008**, *112*, 3469–3481.
37. Liu, Y.; Tarboton, D.; Maidment, D. Height Above Nearest Drainage (HAND) and Hydraulic Property Table for CONUS - Version 0.21 (20200601) 2020.
38. Helsel, D.R.; Hirsch, R.M. *Statistical Methods in Water Resources*; 2002;
39. Scrucca, L. GA: A Package for Genetic Algorithms in R. *Journal of Statistical Software* **2013**, *53*, 1–37.
40. Deb, K.; Pratap, A.; Agarwal, S.; Meyarivan, T. A Fast and Elitist Multiobjective Genetic Algorithm: NSGA-II. *IEEE transactions on evolutionary computation* **2002**, *6*, 182–197.
41. Johnson, J.M. AHGestimation: Tools for Estimating Physically-Based, Computationally Efficient Feature Based Hydraulic Geometry and Rating Curves 2022.
42. Mersmann, O. *Mco: Multiple Criteria Optimization Algorithms and Related Functions*; 2020;
43. Demas, A. *HydroAdd - Linking Water Data to the Stream Network Has Never Been Easier*; USGS, 2022;
44. Blodgett, D.L.; Johnson, J.M. NhdplusTools: Tools for Accessing and Working with the NHDPlus 2022.
45. Ord, J.; Cliff, A. Spatial Autocorrelation. *London: Pion* **1973**.
46. Li, H.; Calder, C.A.; Cressie, N. Beyond Moran's I: Testing for Spatial Dependence Based on the Spatial Autoregressive Model. *Geographical Analysis* **2007**, *39*, 357–375, doi:10.1111/j.1538-4632.2007.00708.x.
47. Moran, P.A.P. Notes on Continuous Stochastic Phenomena. *Biometrika* **1950**, *37*, 17, doi:10.2307/2332142.
48. Afshari, S. USGS AHG Parameters and Supplementary Data 2020.
49. Afshari, Shahab USGS Table AHG Parameters And Supplementary Data 2019.
50. Andreadis, K.M.; Schumann, G.J. Estimating the Impact of Satellite Observations on the Predictability of Large-Scale Hydraulic Models. *Advances in water resources* **2014**, *73*, 44–54.
51. Regan, R.S.; Markstrom, S.L.; Hay, L.E.; Viger, R.J.; Norton, P.A.; Driscoll, J.M.; LaFontaine, J.H. *Description of the National Hydrologic Model for Use with the Precipitation-Runoff Modeling System (PRMS)*; 2018;
52. Brakenridge, G.R. Global Active Archive of Large Flood Events. Dartmouth Flood Observatory, University of Colorado, USA. 2022.
53. Godbout, L.; Zheng, J.Y.; Dey, S.; Eyelade, D.; Maidment, D.; Passalacqua, P. Error Assessment for Height above the Nearest Drainage Inundation Mapping. *JAWRA Journal of the American Water Resources Association* **2019**, *55*, 952–963.
54. Zheng, X.; Maidment, D.R.; Tarboton, D.G.; Liu, Y.Y.; Passalacqua, P. GeoFlood: Large-Scale Flood Inundation Mapping Based on High-Resolution Terrain Analysis. *Water Resources Research* **2018**.
55. Garousi-Nejad, I.; Tarboton, D.G.; Aboutalebi, M.; Torres-Rua, A.F. Terrain Analysis Enhancements to the Height Above Nearest Drainage Flood Inundation Mapping Method. *Water Resources Research* **2019**, *55*, 7983–8009, doi:10.1029/2019WR024837.